SANDIA REPORT
SAND2022-12459
Printed September 2021

Sandia National Laboratories

Physics-Based Optical Neuromorphic Classification

François Léonard, Corinne Teeter, Craig Vineyard

Prepared by
Sandia National Laboratories
Albuquerque, New Mexico
87185 and Livermore,
California 94550

Issued by Sandia National Laboratories, operated for the United States Department of Energy by National Technology & Engineering Solutions of Sandia, LLC.

Available to DOE and DOE contractors from
U.S. Department of Energy
Office of Scientific and Technical Information
P.O. Box 62
Oak Ridge, TN 37831

Telephone: (865) 576-8401
Facsimile: (865) 576-5728
E-Mail: reports@osti.gov
Online ordering: http://www.osti.gov/scitech

Available to the public from
U.S. Department of Commerce
National Technical Information Service
5301 Shawnee Rd
Alexandria, VA 22312

Telephone: (800) 553-6847
Facsimile: (703) 605-6900
E-Mail: orders@ntis.gov
Online order: https://classic.ntis.gov/help/order-methods/

ABSTRACT

Typical approaches to classify scenes from light convert the light field to electrons to perform the computation in the digital electronic domain. This conversion and downstream computational analysis require significant power and time. Diffractive neural networks have recently emerged as unique systems to classify optical fields at lower energy and high speeds. Previous work has shown that a single layer of diffractive metamaterial can achieve high performance on classification tasks. In analogy with electronic neural networks, it is anticipated that multilayer diffractive systems would provide better performance, but the fundamental reasons for the potential improvement have not been established. In this work, we present extensive computational simulations of two-layer diffractive neural networks and show that they can achieve high performance with fewer diffractive features than single layer systems.

CONTENTS

Abstract 3
Acronyms and Terms 7
1. Introduction 8
1.1. System ..... **Error! Bookmark not defined.**
References 13
Distribution ..... **Error! Bookmark not defined.**

LIST OF FIGURES

Figure 1. Geometry of the free-space diffractive neural network. (Left) The source light field propagates to a material consisting of subwavelength apertures. Each aperture is partially filled with a dielectric material, as shown in cross-section. Secondary waves are emitted from each aperture, with a phase ϕ_k determined by the thickness of the dielectric material in aperture *k*. (Right) The source light is constructed from the 28x28 pixels of the dataset, as illustrated with the handwritten number 5. The material is of side length *L* and aperture spacing *d* on a square array. The different dielectric thicknesses for each aperture are illustrated with colorized circles to facilitate visualization. The detector plane has ten detectors, with one detector in the middle and the other nine arranged in a circle of radius *R*..... 10
Figure 2. Testing accuracy for MNIST as a function of the total number of apertures for single layer and two-layer systems. The data points for the single layer system are the best optimized results previously obtained from our simulations. The data points in orange for the two-layer system are all the data points obtained for different values of the separation between the planes and the last plane and the detector plane. The blue data points are the best results for the two-layer system..... 11

This page left blank

ACRONYMS AND TERMS

Acronym/Term	*Definition*
DNN	*Diffractive Neural Network*

1. INTRODUCTION

Identifying features in a scene from their emitted or reflected light is at the core of many applications such as autonomous driving, feature recognition, and imaging. Usually this is accomplished by analyzing digital images captured by photodetectors with high-end algorithms running on electronic computers. An alternative approach has recently emerged whereby passive optical materials that diffract free-space optical fields act as neural networks and perform neuromorphic inference[1-3] without relying on computation in the electronic domain. This all-optical approach has potential for significant improvements in speed and energy consumption by taking advantage of the physics of light propagation. Hybrid approaches have also been explored where free-space optical front ends are integrated with electronic neural networks [4, 5] such that the optical material replaces some part of the neural network, most commonly the convolution layer.

Recently, we presented detailed studies of *single-layer* diffractive neural networks (DDNs) and established the conditions under which high performance can be achieved through optimization. However, it is well-known that electronic neural networks benefit from depth, i.e. multiple successive layers process the information to perform classification. Initial work in DNNs indicated that multiple layers performed significantly better than a single layer, but later research has since demonstrated that single layers can also achieve high performance. Thus, there is an open question as to whether DNNs benefit from depth, and if so in what manner. This is particularly true given that in electronic neural networks depth is usually accompanied with nonlinearity at each layer, a feature that is not present in standard DNNs.

In this manuscript we present extensive numerical simulations of two-layer DNNs and show that they can achieve high performance with fewer diffractive features than a single layer. We also show that co-design is essential to achieve high performance through co-optimization of materials, architecture, and algorithms.

2. SYSTEM AND MODELING APPROACH

The optical classification system is illustrated in Fig.1. An incoming coherent light field of wavelength λ impinges on two metamaterials (labelled $i = 1, 2$) of size $L_i \times L_i$ consisting of N_i apertures arranged in a square grid (aperture spacing d so that $L_i = \sqrt{N_i}\, d$). Light transmission occurs only through the apertures, labelled $k = 1, ..., N_i$ and located at $\vec{r}_{ki} = (x_k, y_k, z_i)$. Each aperture is filled with a material of refractive index n and thickness t_{ki} so that the transmitted light acquires a phase $\phi_{ki} = 2\pi n t_{ki} / \lambda$ as it transmits through the aperture. The source plane is located at a distance H_{in} from the first material plane, the two material planes are separated by H_{12} while the detector plane is separated from the last material plane by H_{out}. In this work we consider aperture diameters less than the wavelength such that the input light intensity is uniform across the aperture.

The input light field is constructed from the individual digital images of the MNIST dataset. Each digital image consists of $N_{in} \times N_{in} = 28 \times 28$ greyscale pixels which we label with the indices m,n and positions $\vec{r}_{mn} = (ma, na, -H_{in})$ where a is the width of the pixel (see Fig. 1). Throughout this manuscript we set $N_{in} a = L_1$, i.e. the input light fills the first material fully. We construct a continuous monochromatic light field of wavelength λ from the digital images, by considering each pixel of the digital image as a point source of intensity I_{mn} and propagating the light from each pixel as a spherical wave to the material plane.

The amplitude of the input electric field from any given pixel m,n at an aperture in the first material layer is $E_{in}^{mn}(\vec{r}_{k1}) = \sqrt{I_{mn}}\left[(x_{k1} - ma)^2 + (y_{k1} - na)^2 + H_{in}^2\right]^{-1/2}$ and the amplitude of the output field after the first layer is given by

$$E_{out}^{k1,mn}(\vec{r}) = E_{in}^{mn}(\vec{r}_{k1}) \frac{z}{|\vec{r} - \vec{r}_{k1}|^2} \left(\frac{1}{2\pi |\vec{r} - \vec{r}_{k1}|} - \frac{i}{\lambda} \right) e^{i\left(\frac{2\pi}{\lambda}|\vec{r} - \vec{r}_{k1}| + \phi_{k1}\right)}. \quad (1)$$

This equation for the far field is appropriate when the detector plane is several wavelengths from the material plane. (As discussed below, we also use it for closer separations to illustrate the general behavior of the system). In addition, Eq. (1) assumes that the input light field $E_{in}^{mn}(\vec{r}_{k1})$ is uniform across the aperture; this requires that the aperture diameter be less than the wavelength.

Light from the apertures of the first layer described by Eq. (1) propagates to the second layer and serves as the input for the apertures in that layer; the output field after the second layer is

$$E_{out}^{k2,mn}(\vec{r}) = E_{out}^{k1,mn}(\vec{r}_{k2}) \frac{z}{|\vec{r} - \vec{r}_{k2}|^2} \left(\frac{1}{2\pi |\vec{r} - \vec{r}_{k2}|} - \frac{i}{\lambda} \right) e^{i\left(\frac{2\pi}{\lambda}|\vec{r} - \vec{r}_{k2}| + \phi_{k2}\right)}. \quad (1.2)$$

Since the light is coherent, the total time-averaged output intensity at detector p is $I_p = \left| \sum_k \sum_{mn} E_{out}^{k,mn}(\vec{r}_p) \right|^2$. To identify objects from the light field we first consider the case of M output photodetectors, each corresponding to one of the M classes. The detectors are distributed in a circular pattern on a plane, as illustrated in Fig. 1, with $\vec{r}_p$ denoting the position of detector p, with p = 0,…9. We chose the digit "0" (item 1 for Fashion) for the center detector and evenly distributed the remaining nine detectors around the circle. Other arrangements are also possible. For example, previous work has considered square distributions[1, 6, 7], and it might be possible to reduce the number of detectors using a combinatorial detection scheme. Further work is needed to determine the optimal detector configuration. The detector pattern radius chosen here was previously shown to be optimal for a single layer[8].

The approach is to learn the phases ϕ_{ki} such that the intensity on detector p is maximal when the incoming light field contains an object corresponding to class p. This is done by minimizing the cross-entropy cost function

$$C = -\frac{1}{N}\sum_{images} \log\left(\frac{e^{\tilde{I}_t}}{\sum_{p=1}^{M} e^{\tilde{I}_p}}\right) \tag{3}$$

where the sum is over the N training images, and the subscript t indicates the target detector. This standard function is chosen because it provides good accuracy and convergence for classification tasks on MNIST when used with electronic neural networks[9]. We normalized the intensities[2] as

$$\tilde{I}_p = f\frac{I_p}{\max\{I\}} \tag{4}$$

where $\max\{I\}$ means the maximum value of the intensity on the M detectors. In this work we use $f=10$ since it gave good performance for single layers.

Datasets and training. We use a gradient descent approach with the Adam algorithm [10], with the learning rate halved if the training accuracy decreased between two successive epochs (defined as one pass through the full training dataset). The phases were updated at each epoch using the analytical expressions for. The process was implemented in Fortran MPI and distributed on up to 100 parallel processors (2.6 GHz, 64GB of RAM).

The MNIST[11] dataset was used in its original format and order. MNIST images correspond to the handwritten digits 0 to 9, and we therefore used 10 detectors on the output plane. We trained on the first 50,000 images and tested on 10,000 images. The phases were optimized using mini-batches of 50 images. The inference performance was obtained by calculating the optical intensity on each of the output detectors, with a successful classification when the output light intensity was maximal on the target detector.

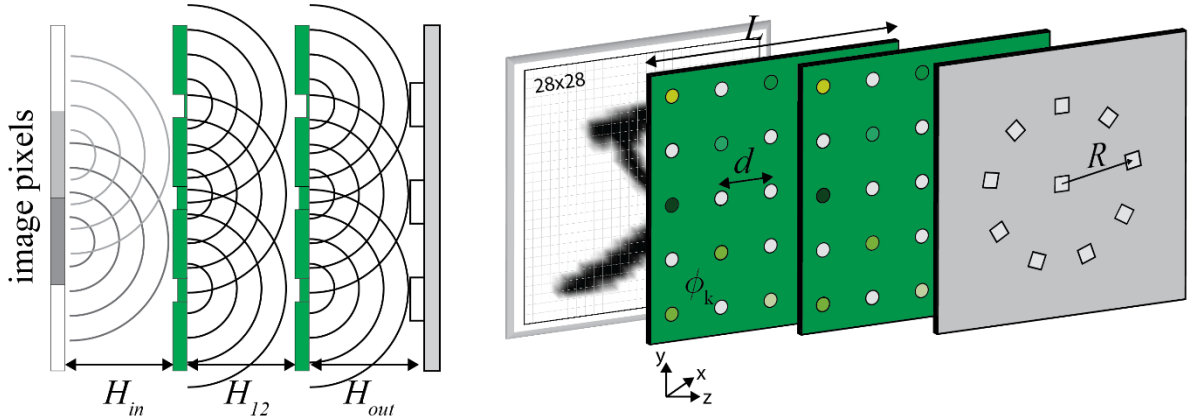

Figure 1. Geometry of the free-space diffractive neural network. (Left) The source light field propagates to a material consisting of subwavelength apertures. Each aperture is partially filled with a dielectric material, as shown in cross-section. Secondary waves are emitted from each aperture, with a phase ϕ_{ki} determined by the thickness of the dielectric material in aperture k. (Right) The source light is constructed from the 28x28 pixels of the dataset, as illustrated with the handwritten number 5. The material is of side length L and aperture spacing d on a square array. The different dielectric thicknesses for each aperture are illustrated with colorized circles to facilitate visualization. The detector plane has ten detectors, with one detector in the middle and the other nine arranged in a circle of radius R.

3. RESULTS

The main result of this work is shown in Fig. 2. There, the testing error on the MNIST dataset is plotted as a function of the total number of apertures in the system, comparing the case of two layers with a single layer. Our results for two layers qualitatively follow those for a single layer: for a small number of apertures N, the testing error decreases as 1/N, until it reaches about 6%, after which further increases in N only lead to slow decrease of the testing error. The advantage of the two-layer system is seen for testing errors greater than ~5%, where the number of apertures to achieve a certain error is lower for the two-layer system compared to the single layer system. For example, the single layer system requires about 1400 apertures to achieve 5% error, while the two layer system only needs about 450. Interestingly, as the number of apertures increases both systems seem to follow the same quantitative behavior, with lowest error of about 4%.

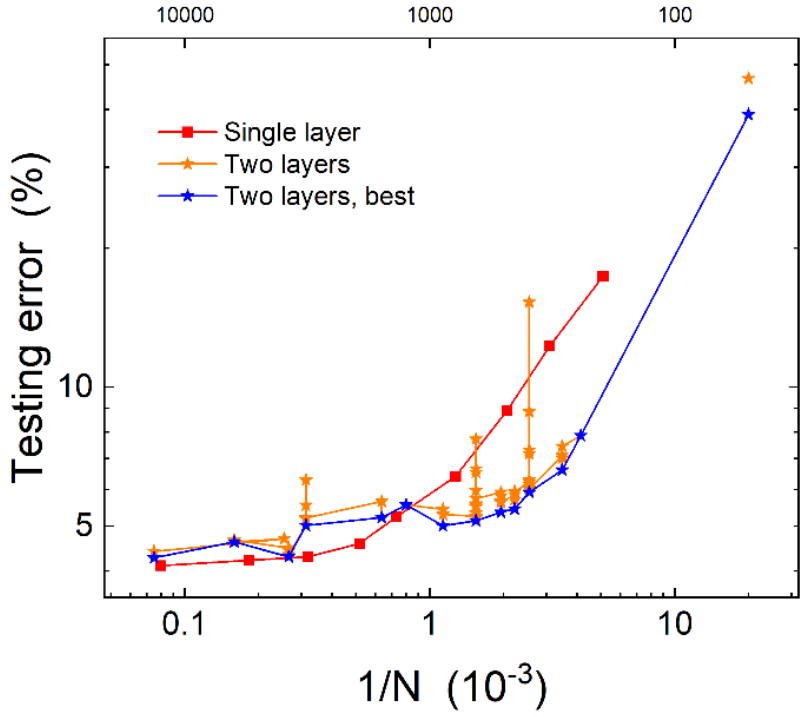

Figure 2. Testing accuracy for MNIST as a function of the total number of apertures for single layer and two-layer systems. The data points for the single layer system are the best optimized results previously obtained from our simulations. The data points in orange for the two-layer system are all the data points obtained for different values of the separation between the planes and the last plane and the detector plane. The blue data points are the best results for the two-layer system.

Figure 2 also shows several data points for each total number of apertures for the two-layer system. Each data point was obtained by training the system for fixed values of H_{12} and H_{out}. One can see that significant variations in the testing error are found for the same number of apertures, even though each point was fully trained. This behavior was previously described for a single layer case where the importance of co-designing the system was found to be critical to achieve high performance. The two-layer system also shows this behavior, with even more complexity since the number of physical parameters to optimize is larger.

4. CONCLUSION

Diffractive neural networks are attracting interesting for their ability to perform classification tasks with reduced energy and at faster speeds. Determining their full potential requires an assessment of key factors such as the impact of depth on performance. In this work, we showed that extending DNNs from a single to two layers can lead to a significant reduction in the number of needed features to achieve a given accuracy. However, we find that even after careful optimization, adding depth does not lead to improved performance for a large number of features. These results pose interesting questions about the fundamental computing capacity of DNNs, and how it can be harnessed in actual physical systems.

REFERENCE

1. Lin, X., et al., *All-optical machine learning using diffractive deep neural networks.* Science, 2018. **361**(6406): p. 1004-1008.
2. Mengu, D., et al., *Analysis of Diffractive Optical Neural Networks and Their Integration With Electronic Neural Networks.* IEEE Journal of Selected Topics in Quantum Electronics, 2020. **26**(1): p. 1-14.
3. Wu, Z., et al., *Neuromorphic metasurface.* Photonics Research, 2020. **8**(1): p. 46-50.
4. Colburn, S., et al., *Optical frontend for a convolutional neural network.* Applied Optics, 2019. **58**(12): p. 3179-3186.
5. Burgos, C.M.V., et al., *Design framework for metasurface optics-based convolutional neural networks.* Applied Optics, 2021. **60**(15): p. 4356-4365.
6. Chang, J., et al., *Hybrid optical-electronic convolutional neural networks with optimized diffractive optics for image classification.* Scientific Reports, 2018. **8**(1): p. 12324.
7. Zhou, T., et al., *Large-scale neuromorphic optoelectronic computing with a reconfigurable diffractive processing unit.* Nature Photonics, 2021. **15**(5): p. 367-373.
8. Léonard, F., et al., *Co-Design of Free-Space Metasurface Optical Neuromorphic Classifiers for High Performance.* ACS Photonics, 2021. **8**: p. 2103-2111.
9. Janocha, K. and W.M. Czarnecki, *On Loss Functions for Deep Neural Networks in Classification.* Schedae Inform., 2016. **25**: p. 49-59.
10. Kingma, D.P. and J. Ba, *Adam: A method for stochastic optimization.* 2014: p. arXiv:1412.6980 [cs.LG]
11. Lecun, Y., et al., *Gradient-based learning applied to document recognition.* Proceedings of the IEEE, 1998. **86**(11): p. 2278-2324.

DISTRIBUTION

Email—Internal

Name	*Org.*	*Sandia Email Address*
John Feddema	*1460*	*jtfedde@sandia.gov*
Technical Library	*1911*	*sanddocs@sandia.gov*

This page left blank

Sandia National Laboratories is a multimission laboratory managed and operated by National Technology & Engineering Solutions of Sandia LLC, a wholly owned subsidiary of Honeywell International Inc. for the U.S. Department of Energy's National Nuclear Security Administration under contract DE-NA0003525.